PAPER

Check for updates

Perylene diimide-based supramolecular polymer with temperature-sensitive ratiometric fluorescence responsiveness in solution and gels†

Jie Liu,[a] Yubing Zhang,[a] Chonghua Zhang,[a] Peisheng Zhang, [ID][a] Rongjin Zeng,*[a] Jiaxi Cui [ID]*[b] and Jian Chen [ID]*[ac]

A novel amphiphilic fluorescence building block with perylene diimide (PDI) as the core and quadruple H-bonding groups (UPy) as wings (UPy–PDI–UPy) has been synthesized. It shows interesting thermo-responsive ratiometric dual-emission properties in both aqueous solution and the hydrogel state. Further contrast experiments with two other analogous derivatives, namely UPy–TPDI–UPy and TEG–PDI–TEG, indicated that the presence of supramolecular aggregation induced an emission enhancement effect between the UPy–PDI–UPy molecules, attributed to the synergetic effect of intermolecular intrinsic π–π stacking, the hydrophobic effect and highly directional quadruple H-bonding. In DMF/H_2O (v : v = 1 : 1), UPy–PDI–UPy self-assembles into nanoparticles with obvious ratiometric fluorescence responsiveness towards temperature in the range of 20–80 °C. Moreover, UPy–PDI–UPy can form a thermo-responsive hydrogel by dispersing in PEG-containing aqueous solution. The hydrogels show a temperature-dependent ratiometric dual-emission with a narrow responsive range of 20–39 °C and an excellent renewable property. This innovative research helps to fabricate novel responsive luminescent materials by using the supramolecular self-assembly behavior.

Introduction

Temperature-sensitive fluorescent materials are attracting increasing attention due to their application potential in fields from biosensing to information encryption.[1–4] In these applications, ratiometric fluorescence is preferred because it provides high resolution and allows accurate and quantitative readout in combination with a simple fluorescence change.[5–15] Different material systems have been developed to get thermo-sensitive ratiometric fluorescence, including hybrid nanoparticles, carbon dots, polymer systems, rare-earth complexes, *etc.*[10–15]

[a] *Key Laboratory of Theoretical Organic Chemistry and Functional Molecule of Ministry of Education, Hunan Provincial Key Laboratory of Controllable Preparation and Functional Application of Fine Polymers, Hunan Provincial Key Lab of Advanced Materials for New Energy Storage and Conversion, School of Chemistry and Chemical Engineering, Hunan University of Science and Technology, Xiangtan, Hunan, 411201, China. E-mail: zengrj1963@126.com, cj0066@gmail.com; Fax: +86 731 58290045; Tel: +86 731 58290045*

[b] *Institute of Fundamental and Frontier Sciences, University of Electronic Science and Technology of China, Chengdu, Sichuan, 610054, China. E-mail: jiaxicui119@gmail.com*

[c] *State Key Laboratory of Luminescent Materials and Devices, South China University of Technology, Guangzhou 510640, P. R. China*

† Electronic supplementary information (ESI) available: Synthesis procedures, ^{1}H NMR spectra, ^{13}C NMR, MS, absorption spectrum, fluorescence spectra, *etc.*. See DOI: 10.1039/d0ma00053a

These systems either require complicated fabrication processes and extra calibration of physicochemical properties between the two different components or are unstable in polar solvents and show remarkable fluorescence quenching to oxygen.[10–15] Fabricating ratiometric fluorescence thermo-sensing materials with single-component dyes could be a good solution to overcome these disadvantages. However, the design of such dyes is very challenging due to Kasha's rule.

The integration of dyes into a supramolecular system is an efficient method to create thermo-sensitive fluorescence materials.[16–18] Among various supramolecular systems, supramolecular assemblies based on multiple H-bonding interactions have been proven to be a promising way to construct novel fluorescent supramolecular polymers with controllable, stimuli-responsive, and reversible features.[16–23] In these systems, the fluorophore moieties are conjugated with the H-bonding units to form fluorescence building blocks.[16–23] When the temperature lowers to allow the formation of directional H-bonding to order the fluorophores, the materials normally show weak fluorescence due to the quenching effect.[24] It is difficult to obtain ratiometric fluorescence, especially for the normal fluorophores that show obvious aggregation-caused quenching (ACQ) in the solid-state or high concentration of solution.

Perylene diimide (PDI) is one of the most well-known fluorescent building blocks to fabricate supramolecular

fluorescence materials.[25] It has been identified as an ideal candidate for fabricating organic optoelectronic devices, dye lasers, optical switches, and fluorescent sensors.[25–31] And it exhibits numerous appealing features including easy functionalization, excellent stability, and ultrahigh fluorescence quantum yields in the molecular state.[32–35] In spite of these advantages, traditional PDI-based supramolecular materials usually suffer from relatively weak fluorescent intensities of redshift emission, low quantum yields, and undesirable ACQ in aggregated states due to the strong intermolecular π–π stacking of the PDI plane.[36–39] Thus, the optimization of the supramolecular structure to modulate the π–π stacking of PDI is essential to achieve bright emission in the aggregated state, which can be realized by the introduction of various aromatic rings as isolation groups from the sides.[37,38] However, this strategy is often hindered by the complicated synthesis routes, and the obtained dyes generally exhibit a stationary red or deep red emission nature.[40,41]

Herein we report our strategy to prepare PDI-based ratiometric fluorescence supramolecular materials that are thermosensitive. In our strategy, the highly directional quadruple hydrogen bonding units of ureidopyrimidinone (UPy) are designed to conjugate with PDI to control the intermolecular π–π stacking for endowing the dye with bright red emission in the aggregated state, together with a temperature-dependent ratiometric fluorescence property. We demonstrate this concept by comparing three rationally designed amphiphilic PDI derivatives, UPy–PDI–UPy, UPy–TPDI–UPy and TEG–PDI–TEG (Scheme 1), which are composed of a hydrophobic PDI core and two hydrophilic wings. Thanks to the unsubstituted core and linked quadruple H-bonding group (UPy) as wings, only the supramolecular polymer UPy–PDI–UPy exhibited an intense fluorescence emission in the solid-state and a temperature-dependent ratiometric dual-emission (green and red) property

in the nanoparticle dispersion when temperature increased from 20 to 80 °C. It is noteworthy that the subsequently prepared fluorescent hydrogel displayed a temperature-ultrasensitive ratiometric fluorescence responsiveness and a visual sol–gel transition ranging from 20 to 39 °C. To the best of our knowledge, this is the first example of the fabrication of PDI-based supramolecular polymers as ratiometric fluorescence thermometers and can imply more inspiration to prepare novel responsive luminescent materials (Scheme 1).

Experimental

Materials and methods

Unless otherwise stated, all the chemicals were purchased from commercial sources and directly used in the reaction. The detailed synthesis routes of relevant intermediates such as UPy-SH, OH–PDI–OH (**2a**) and OH–TPDI–OH (**2b**), as well as the final products including UPy–TPDI–UPy and TEG–PDI–TEG (Schemes S1–S3, ESI†), and the relevant apparatus and characterization including NMR spectra, mass spectra (MS), UV-vis absorption and fluorescence spectra, fluorescence lifetime, atomic force microscopy (AFM) and control experiments are displayed in the ESI.†

Synthesis of 3a

To a solution of **2a** (742 mg, 1 mmol) in 500 mL dry CH_2Cl_2 (DCM, 4 Å activated molecular sieves, 3 days) at 0 °C, acryloyl chloride (109 mg, 1.2 mmol) and dry triethylamine (NaOH, pellets 3 days) (0.5 mL, 3.6 mmol) were added. The reaction mixture was stirred for 2 h at 0 °C, and kept overnight at room temperature (RT) under an argon atmosphere. After the evaporation of the solvent, the product was purified by gel chromatography using CH_2Cl_2/CH_3OH (50 : 1, v/v). **3a**, a red solid, was obtained in 36% yield (286 mg). ^1H NMR (500 MHz, $CDCl_3$), δ: 8.61 (d, 4H), 8.54 (d, 4H), 6.38 (d, 2H), 6.13 (q, 2H), 5.83 (d, 2H), 4.47 (t, 4H), 4.27 (t, 4H), 3.87 (t, 4H), 3.70–3.61 (m, 20H).

Synthesis of UPy–PDI–UPy

A mixture of **3a** (152 mg, 0.18 mmol), UPy-SH (170 mg, 0.54 mmol) and triethylamine (0.2 mL 1.44 mmol) in CH_2Cl_2 (30 mL) was stirred under N_2 at room temperature for 24 h. After the evaporation of the solvent, the product was purified by gel chromatography using CH_2Cl_2/CH_3OH (100 : 1, v/v) as the eluent to afford UPy–PDI–UPy (120 mg). Yield: 45%. ^1H NMR (500 MHz, $CDCl_3$), δ: 13.06–12.87 (m, 2H), 11.79–11.26 (m, 2H), 10.33–10.07 (m, 2H), 8.53–8.17 (m, 8H), 5.76–5.62 (m, 2H), 4.44 (t, 4H), 4.23 (t, 4H), 3.86 (t, 4H), 3.68–3.62 (m, 20H), 3.40–3.24 (m, 4H), 2.82–2.59 (m, 12H), 2.28 (m, 2H), 1.61–1.25 (m, 16H), 0.89–0.82 (m, 12H). MS (ESI): m/z 1745.6 [M]$^+$ (Fig. S1–S3, ESI†).

Results and discussion

Synthesis and characterization of PDI derivatives

The chemical structures of the designed PDI derivatives are shown in Scheme 1. TEG–PDI–TEG consists of a PDI core and
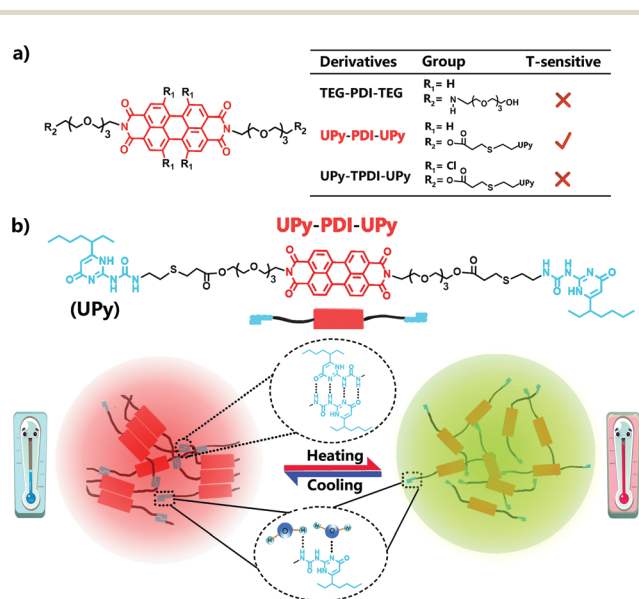
Scheme 1 (a) Molecular structure of three PDI derivatives; 2. (b) Schematic illustration of temperature-sensitive supramolecular fluorescent nano-assemblies.

two hydrophilic 2-[2-[2-(2-aminoethoxy)ethoxy]ethoxy]ethanol (TEG) wings. UPy–PDI–UPy is made from a TEG–PDI–TEG structure and two ureido-4-pyrimidinone (UPy) terminal groups. Such a structure allowed UPy–PDI–UPy to form supramolecular polymers via the self-complementary quadruple H-bonding between the UPy moieties.[18,19] Compared to UPy–PDI–UPy, UPy–TPDI–UPy has a tetrachloro-substituted PDI core. The substituted groups in TPDI were designed to weaken the π–π stacking interaction of the PDI core.[42,43] These PDI derivatives were synthesized by coupling TEG/UPy with bis-*N*,*N*′-(2-(2-(2-(2-hydroxyethoxy)ethoxy)ethoxy)ethyl)-3,4,9,10-perylenetetra-carboxylic diimide (OH–PDI–OH) or bis-*N*,*N*′-(2-(2-(2-(2-hydroxyethoxy)-ethoxy)ethoxy)ethyl)-1,6,7,12-tetrachlorol-3,4,9,10-perylenetetra-carboxylic diimide (OH–TPDI–OH). The detailed synthesis pathways are described in the supporting information. The molecular structure of the three compounds and their inter-mediate products was confirmed by NMR spectra and mass spectra (Fig. S1–S8, ESI†). All the three target molecules obtained exhibit good solubility in some organic solvents including dimethylformamide (DMF), dichloromethane (DCM), tetrahydro-furan (THF), etc., and in DMF/H2O mixed solvent (in either molecular dispersion or aggregation state), due to the presence of the long hydrophilic chains.

Fig. 1 shows the fluorescent properties of the three PDI derivatives in the solid-state. Interestingly, under 365 nm light irradiation, UPy–PDI–UPy emits a bright red light with a high fluorescence quantum yield of 7.19% while both PEG–PDI–PEG and UPy–TPDI–UPy show weak fluorescence with low fluores-cence quantum yields of 0.19% and 0.26%, respectively (Fig. 1a). Such a unique property is supported by their fluores-cence spectra (Fig. 1b) in which the maximum fluorescence emission intensity of UPy–PDI–UPy in the solid state at 694 nm is 53 times or 41 times higher than those of TEG–PDI–TEG at 693 nm or UPy–TPDI–UPy at 636 nm. The absence of emission in both PEG–PDI–PEG and UPy–TPDI–UPy was attributed to the ''aggregation-caused quenching'' (ACQ) effect. It is well documented that the fluorescence of PDIs is generally quenched in the solid-state due to consecutive π–π interactions and/or dipole–dipole interactions between the neighboring planar PDI fluorophores.[39] Würthner and co-workers have demonstrated that bulky substituents on the PDI fluorophore favor the formation of discrete PDI–PDI π-dimers and undis-torted planar PDI fluorophores, which inhibit long-range PDI

aggregation in the solid state.[44,45] As displayed in the ^{1}H NMR spectrum in Fig. S9 (ESI†), with increasing the concentration of UPy–PDI–UPy, the peaks at 8.2 and 8.4 ppm that belong to the PDI–PDI π-dimers gradually rise, indicating that the bulky UPy side groups in UPy–PDI–UPy can lead to the formation of discrete PDI–PDI π-dimers.[46,47] Also, no chemical shifts related to trimers or other long-range PDI aggregation can be observed in Fig. S9 (ESI†). We thus attribute the bright deep-red emission efficiency of UPy–PDI–UPy in the solid state to the appropriate π–π stacking of PDI induced by UPy dimerization.

Because of their amphiphilic structures, the PDI derivatives could self-assemble in aqueous solutions. UV-vis absorption and fluorescence spectroscopies were used to study their self-assemblies (Fig. 2). A DMF/H2O mixture solvent was employed by increasing the fraction of water in DMF. At a concentration of 50 μM, UPy–PDI–UPy completely dissolved in pure DMF, showing typical absorption and emission images of well-dispersed PDI derivatives (Fig. 2a and b).[48,49] When the content of water was increased to 30 vol%, dramatic changes in both the absorption and emission spectra were observed. The $S_{0–1}$ transition ($\lambda = 490$ nm) is more intense than the $S_{0–0}$ transition ($\lambda = 525$ nm) while the fluorescent intensity at around 545 nm is significantly reduced, indicating a π–π stacking aggregation state. With further increase of the water fraction, a slight bathochromic shift of λ_{max} occurred and the well-structured absorption curve turned into a less structured peak. The absorbance ratio of A_{525}/A_{490} was declined from 1.6 to 0.4 (Fig. S10a, ESI†), indicating enhanced π–π stacking interaction.[48] Interestingly, with
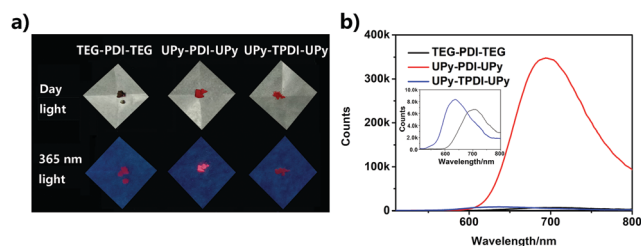
Fig. 1 (a) Photographs of TEG–PDI–TEG, UPy–PDI–UPy and UPy–TPDI–UPy powder under daylight and 365 nm UV irradiation. (b) The corresponding fluorescence emission spectra of three molecules in the solid-state. $\lambda_{ex} = 490$ nm.
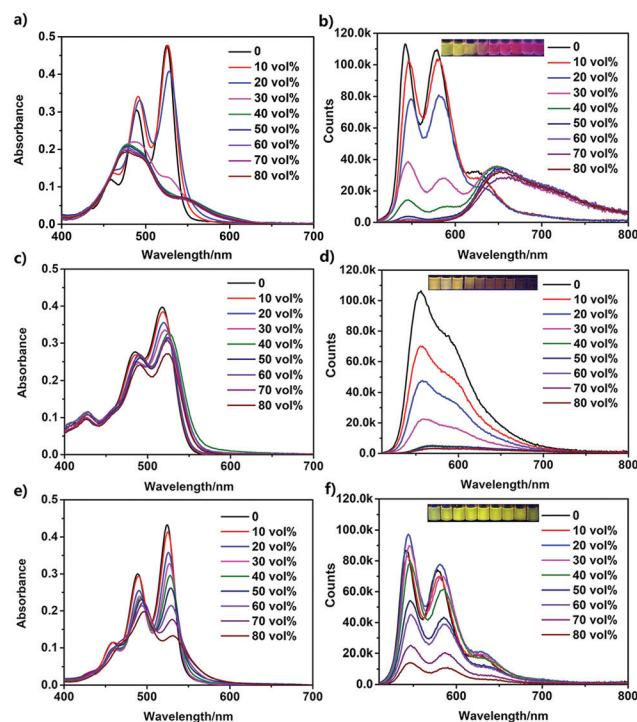
Fig. 2 UV-vis and fluorescence emission spectra of UPy–PDI–UPy (a and b), UPy–TPDI–UPy (c and d) and TEG–PDI–PDI–TEG (e and f) in different water fractions of DMF/H2O mixed solution (50 μM), respectively. Fluores-cence emission spectra: $\lambda_{ex} = 490$ nm.

a further increase of water fraction, UPy–PDI–UPy shows a significant enhancement of fluorescence intensity at 646 nm, accompanied by a change of emission color from green to red. This unusual enhancement in emission is different from most previous reports of the PDI derivatives, even UPy-linked ones.[48,49] We attributed this to the formation of appropriate intermolecular π–π stacking through multiple H-bonding interactions. Such a synergetic effect was supported by the results from UPy–TPDI–UPy in which the tetrachloro substituents prevent the intermolecular π–π stacking interaction and TEG–PDI–TEG, a PDI derivative without UPy moieties. UPy–TPDI–UPy only exhibits a slight change in absorption along with the absorbance ratio of A_{518}/A_{490} (Fig. S10b, ESI†), and obvious fluorescence quenching at a higher water fraction (Fig. 2c and 3d). On the other hand, TEG–PDI–TEG shows an obvious decrease in the absorption peak at $S_{0–0}$ transition (Fig. 2e) but a stepwise promotion in that of the $S_{0–1}$ transition. As a result, the absorbance ratio of A_{525}/A_{490} declines from 1.45 to 0.7 (Fig. S10c, ESI†). In addition to this change, clear quenching in fluorescence intensity was observed, due to the formation of strong π–π interaction mediated aggregates, as reported in the literature.

To further investigate the aggregation behavior of UPy–PDI–UPy in DMF/H$_2$O mixed solution, AFM, TEM and DLS were employed to study the size of its aggregatesunder different water fractions. As exhibited in Fig. 3 and Fig. S11 (ESI†), when the water fraction was increased from 20% to 80%, the particle size data from DLS gradually decrease and the size distribution was also reduced. The results were also confirmed by AFM and TEM measurements. Fig. 3a and c display the AFM images of the supramolecular aggregates of UPy–PDI–UPy in DMF/H$_2$O mixed solution with 30% or 50% fraction. In the case of 30% water fraction, the aggregates show an average size of 396.5 nm (DLS). Increasing water fraction reduces both the average particle size and size distribution. The TEM images as shown

in Fig. S12 (ESI†) further confirm the aggregation behavior of UPy–PDI–UPy in the mixture of DMF/H$_2$O. This indicated that solvent polarity can be used to regulate the supramolecular self-assembly behavior of UPy–PDI–UPy in the current system.

Ratiometric fluorescence responsiveness of temperature in solution and gels

Temperature-dependent fluorescence emission spectra of the UPy–PDI–UPy nanoparticle dispersion in DMF/H$_2$O mixed solution (v/v = 50/50) were recorded from 20 °C to 80 °C (Fig. 4). With an increase in temperature, the fluorescence peak at 646 nm decreases and the emission around 545 nm becomes dominant (Fig. 4a). The average lifetime of the dispersion at 646 nm also declines from 15.9 ns to 8.9 ns (Fig. S13, ESI†). The change in emission was attributed to the disassembly of PDI cores associated with both π–π stacking and H-bonding interactions. The absorption spectra of the dispersion as shown in Fig. S14 (ESI†) supported the conclusion that the π–π stacking interaction was reduced with temperature promotion. In this process, particle size was reduced (Fig. S15, ESI†), due to the segmental disaggregation of the formed supramolecular aggregates. Notably, a prominent linear fitting curve, with a correlation coefficient of $R^2 = 0.98$, was also achieved by plotting the logarithm of I_{545}/I_{646} versus temperature (20.0–80.0 °C). This perfect fitting implied that the nanoparticle dispersion can serve as a favorable ratiometric fluorescent sensor for temperature. In addition, when the temperature was alternated between 20 and 80 °C, the nanoparticle dispersion exhibited reversibly switchable fluorescence nature (Fig. 4c). A slight "fatigue" effect was observed in reversibility (Fig. 4c) and fluorescence brightness (Fig. 5d). As shown in Fig. S16 (ESI†), when the
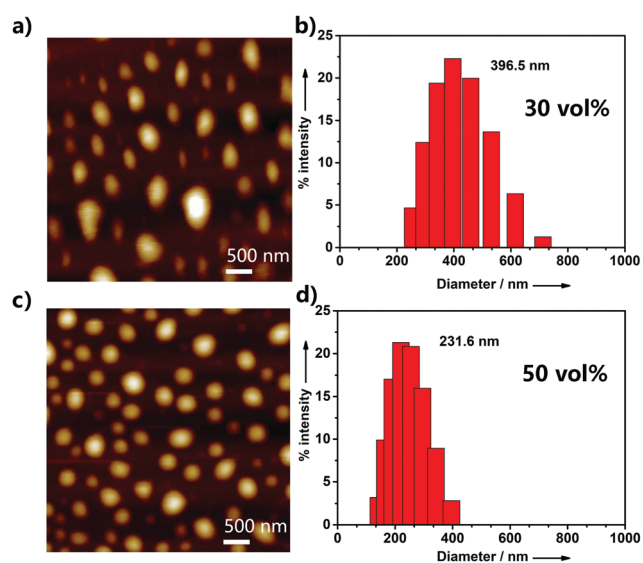

Fig. 3 AFM images and DLS distribution graph of the nanoparticles via the self-assembly of UPy–PDI–UPy (50 μM) in DMF/H$_2$O mixed solution with a water fraction of 30 vol% (a and b) and 50 vol% (c and d), respectively.
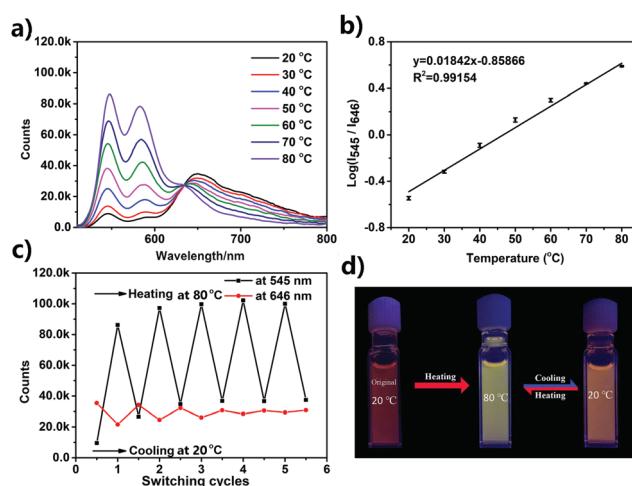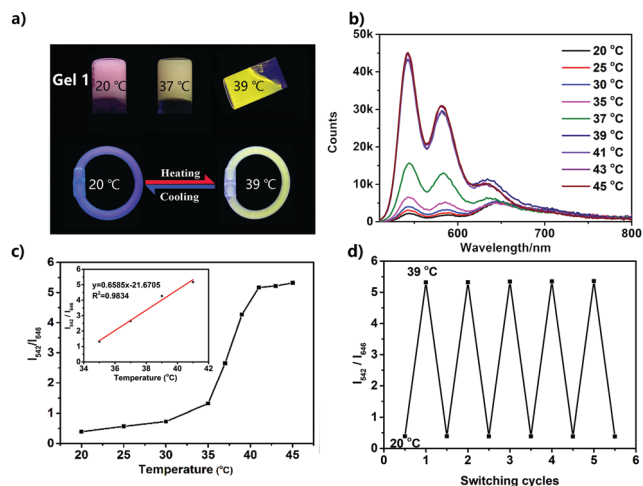

Fig. 4 (a) Temperature dependent fluorescence emission of the UPy–PDI–UPy (50 μM) nanoparticle dispersion in DMF/H$_2$O: 50/50 (v/v). λ_{ex} = 490 nm. (b) The ratiometric fluorescence intensity (I_{545}/I_{646}) of the nanoparticle dispersion versus temperature, as well as the corresponding linear fitting curve. (c) Renewable cycles of the corresponding fluorescence intensity at 546 nm and 649 nm change with cooling at 20 °C and heating at 80 °C. (d) Fluorescence photographs of the nanoparticle dispersion at the first cooling at 20 °C and the switchable fluorescence states between 20 °C and 80 °C.

Fig. 5 (a) Fluorescence photographs of Gel1 at various temperatures, and the temperature-sensitive bracelet made of Gel1. (b) Temperature-dependent fluorescence emission of Gel1. λ_{ex} = 490 nm. (c) The ratiometric fluorescence intensity (I_{542}/I_{646}) of Gel1 versus temperature, and the corresponding linear fitting curve (inset). (d) Switching cycles of the I_{542}/I_{646} of Gel1 between 20 °C and 39 °C.

temperature was decreased from 80 °C to 20 °C, some big UPy–PDI–UPy nanoparticles form, which increases the distribution of nanoparticles. This result is significantly different from that of the nanoparticles formed in the mixture of DMF/H$_2$O solvent (Fig. 3c and d). The different assembly strategies make the color and the fluorescence emission spectra of the nanoparticles (Fig. 4d and Fig. S17, ESI†) different from that of the initial sample at 20 °C. In addition, the "fatigue" emission still exists, even when the incubation time of cooling was prolonged to 46 h (Fig. S17, ESI†). However, marked fluorescent switching can still be visualized after five test cycles. In addition, the photostability of UPy–PDI–UPy nanoparticles in the mixture of DMF/H$_2$O is provided in Fig. S18 (ESI†). The nanoparticles displayed good photostability under the continuous excitation of 490 nm for 60 min. Thus, the nanoparticle dispersion exhibited attractive properties for renewable temperature sensing in various applications.

A UPy–PDI–UPy hydrogel could be prepared by adding polyethylene glycol (PEG, M_w = 10 000) into the solution. This hydrogel (Gel1) was also thermo-sensitive. Elevating the temperature from 20 to 39 °C induced a sol–gel transition (Fig. 5a). Interestingly, Gel1 displays an obvious fluorescence color change from pink to greenyellow, accompanied by the sol–gel transition. The emission was further studied using fluorescence spectroscopy. As displayed in Fig. 5b, UPy–PDI–UPy in a hydrogel (Gel1) exhibits a high thermo-sensitivity in fluorescence, even more sensitive than that in the solution state. The ratiometric fluorescent intensity I_{542}/I_{646} was further used to evaluate the thermo-sensitivity (Fig. 5c). It was found that a sharp change in I_{542}/I_{646} (1.1 to 5.3) occurred in the range of 35–41 °C (critical temperature range). We attribute this to the phase-transition temperature of PEG in the as-prepared hydrogel intensifying the disaggregation of the formed supramolecular aggregates during the phase-transition process. Moreover, a good linear fitting curve with a correlation coefficient of

0.98 (R^2) was achieved by plotting the I_{542}/I_{646} versus temperature (35.0–41.0 °C). Note that this change perfectly matched the human physiological temperature range, implying a potential application in body-monitor devices. A temperature-sensitive color-changing bracelet by the encapsulation of Gel1 in a plastic tube was thus fabricated to show this potential (Fig. 5a). In addition, Gel1 also exhibits excellent reversibility in thermo-induced fluorescence change between 20 and 39 °C (Fig. 5d). In comparison with the corresponding nanoparticle dispersion, no detectable "fatigue" effects were observed in the reversibility even after five cycles. Furthermore, the critical temperature range of the gel can be easily varied by changing the ratio and molecular weight of PEG, as exhibited in Table S1 and Fig. S19–S21 (ESI†). In the current system, PEG is the major component (58 and 75 wt% for Gel1 and Gel2, respectively) and water is absorbed in the PEG as a plasticizer in the gel state. PEG with M_w of 10 000 shows a melting point of ca. 60 °C, which is expected to decrease after the addition of water. The gel–sol transition is the melting of the mixture of PEG and water. This hypothesis is also supported by the system of the PEG with lower M_w (2000). Decreasing the M_w can reduce the melting point of PEG itself and also decrease the transition temperature of the system (system of M_w 10 000: 41 °C; system of M_w 2000: 36 °C). Based on this mechanism, the concentration of PEG should make an important contribution to the phase transition, as the results show in Table S1, Fig. 5a and Fig. S19 (ESI†) (39 °C for Gel1 and 41 °C for Gel2). In this system, the UPy–PDI–UPy molecules disperse in the media and would thus change their aggregated state with the media. Moreover, similar to UPy–PDI–UPy, TEG–PDI–TEG can also form a hydrogel. However, in contrast with the obvious temperature-dependence of UPy–PDI–UPy hydrogel, the corresponding TEG–PDI–TEG in gel (Gel4, Table S1, Fig. S19 and S22, ESI†) did not show any fluorescence color change except for the presence of fluorescence quenching and gel–sol transition with the increase of temperature.

Conclusions

In summary, we have synthesized three amphiphilic PDI derivatives, PEG–PDI–PEG, UPy–PDI–UPy, and UPy–TPDI–UPy. They have a PDI core and PEG/PEG-UPy wings. It was found that UPy–PDI–UPy exhibited an intense deep-red fluorescence emission not only in the solid-state, but also in the nanoparticle dispersion, implying an aggregation-induced-enhancement in fluorescence. We attributed such enhancement in fluorescence to the formation of appropriate π–π stacking. Interestingly, UPy–PDI–UPy in a DMF/H$_2$O mixture solution (the volume ratio of H$_2$O is 50%) displayed obviously ratiometric fluorescence responsiveness against temperature in the range of 20–80 °C, together with a good reversible cycling property. Moreover, the as-prepared fluorescent gels consisting of UPy–PDI–UPy and PEG not only exhibited visual sol–gel transition, but also showed temperature-sensitive ratiometric dual-emission signals at a narrow range of 20–39 °C with excellent renewable nature, which perfectly matched the human physiological temperature range.

Those temperature-dependent ratiometric emission properties suggested potential application in various visual luminescent devices such as anti-counterfeiting labels and ratiometric fluorescent thermometers.

Conflicts of interest

The authors declare no competing financial interest.

Acknowledgements

Notes and references

1 A. Julià López, D. Ruiz-Molina, K. Landfester, M. B. Bannwarth and C. Roscini, *Adv. Funct. Mater.*, 2018, **28**, 1801492.

2 D. H. Liu, Z. B. Sun, Z. H. Zhao, Q. Peng and C. H. Zhao, *Chem. – Eur. J.*, 2019, **25**, 10179–10187.

3 J. Wang, N. Wang, G. Wu, S. Wang and X. Li, *Angew. Chem., Int. Ed.*, 2019, **58**, 3082–3086.

4 Z. Wang, X. He, T. Yong, Y. Miao, C. Zhang and B. Z. Tang, *J. Am. Chem. Soc.*, 2020, **142**, 512–519.

5 W. Zhang, X. Ji, B. J. Peng, S. Che, F. Ge, W. Liu, M. Al-Hashimi, C. Wang and L. Fang, *Adv. Funct. Mater.*, 2019, **30**, 1906463.

6 P. Zhang, H. Wang, Y. Hong, M. Yu, R. Zeng, Y. Long and J. Chen, *Biosens. Bioelectron.*, 2018, **99**, 318–324.

7 X. Peng, Z. Yang, J. Wang, J. Fan, Y. He, F. Song, B. Wang, S. Sun, J. Qu, J. Qi and M. Yang, *J. Am. Chem. Soc.*, 2011, **133**, 6626–6635.

8 H. Wang, P. Zhang, Y. Hong, B. Zhao, P. Yi and J. Chen, *Polym. Chem.*, 2017, **8**, 5795–5802.

9 E. Navarro Ceron, D. H. Ortgies, B. del Rosal, F. Ren, A. Benayas, F. Vetrone, D. Ma, F. Sanz-Rodriguez, J. Garcia Sole, D. Jaque and E. Martin Rodriguez, *Adv. Mater.*, 2015, **27**, 4781–4787.

10 J. Chen, C. Zhang, K. Lv, H. Wang, P. Zhang, P. Yi and J. Jiang, *Sens. Actuators, B*, 2017, **251**, 533–541.

11 C. Wang, H. Lin, Z. Xu, Y. Huang, M. G. Humphrey and C. Zhang, *ACS Appl. Mater. Interfaces*, 2016, **8**, 6621–6628.

12 D. Wang, T. Liu, J. Yin and S. Liu, *Macromolecules*, 2011, **44**, 2282–2290.

13 Y. Takei, S. Arai, A. Murata, M. Takabayashi, K. Oyama, S. I. Ishiwata, S. Takeoka and M. Suzuki, *ACS Nano*, 2014, **8**, 198–206.

14 M. Kamimura, T. Matsumoto, S. Suyari, M. Umezawa and K. Soga, *J. Mater. Chem. B*, 2017, **5**, 1917–1925.

15 L. Li, Y. Zhu, X. Zhou, C. D. S. Brites, D. Ananias, Z. Lin, F. A. A. Paz, J. Rocha, W. Huang and L. D. Carlos, *Adv. Funct. Mater.*, 2016, **26**, 8677–8684.

16 A. Lavrenova, D. W. Balkenende, Y. Sagara, S. Schrettl, Y. C. Simon and C. Weder, *J. Am. Chem. Soc.*, 2017, **139**, 4302–4305.

17 S. Tomohiro, D. Arnab, T. Youichi and S. Seiji, *J. Am. Chem. Soc.*, 2010, **132**, 13928–13935.

18 H. Wang, W. Zhang, X. Dong and Y. Yang, *Talanta*, 2009, **77**, 1864–1868.

19 H. Q. Peng, C. L. Sun, L. Y. Niu, Y. Z. Chen, L. Z. Wu, C. H. Tung and Q. Z. Yang, *Adv. Funct. Mater.*, 2016, **26**, 5483–5489.

20 Y. Y. Huang, Y. Tian, X. Q. Liu, Z. Niu, Q. Z. Yang, V. Ramamurthy, C. H. Tung, Y. Z. Chen and L. Z. Wu, *Mater. Chem. Front.*, 2018, **2**, 1893–1899.

21 J. F. Xu, Y. Z. Chen, D. Y. Wu, L. Z. Wu, C. H. Tung and Q. Z. Yang, *Angew. Chem., Int. Ed.*, 2013, **52**, 9738–9742.

22 X. Zhu, J. X. Wang, L. Y. Niu and Q. Z. Yang, *Chem. Mater.*, 2019, **31**, 3573–3581.

23 H. Q. Peng, J. F. Xu, Y. Z. Chen, L. Z. Wu, C. H. Tung and Q. Z. Yang, *Chem. Commun.*, 2014, **50**, 1334–1337.

24 G. Huang, Y. Jiang, S. Yang, B. S. Li and B. Z. Tang, *Adv. Funct. Mater.*, 2019, **29**, 1900516.

25 F. Wurthner, C. R. Saha-Moller, B. Fimmel, S. Ogi, P. Leowanawat and D. Schmidt, *Chem. Rev.*, 2016, **116**, 962–1052.

26 C. Li and H. Wonneberger, *Adv. Mater.*, 2012, **24**, 613–636.

27 W. Tan, X. Li, J. Zhang and H. Tian, *Dyes Pigm.*, 2011, **89**, 260–265.

28 S. Kaur, M. Kumar and V. Bhalla, *Chem. Commun.*, 2015, **51**, 4085–4088.

29 J. Yang, F. Chen, H. Ran, J. Y. Hu, B. Xiao, A. Tang, X. Wang and E. Zhou, *Macromol. Rapid Commun.*, 2018, **39**, 1700715.

30 L. Yang, W. Gu, L. Lv, Y. Chen, Y. Yang, P. Ye, J. Wu, L. Hong, A. Peng and H. Huang, *Angew. Chem., Int. Ed.*, 2018, **57**, 1096–1102.

31 Q. Zhao, K. Li, S. Chen, A. Qin, D. Ding, S. Zhang, Y. Liu, B. Liu, J. Z. Sun and B. Z. Tang, *J. Mater. Chem.*, 2012, **22**, 15128–15135.

32 D. Ke, A. Tang, C. Zhan and J. Yao, *Chem. Commun.*, 2013, **49**, 4914–4916.

33 A. Wadsworth, M. Moser, A. Marks, M. S. Little, N. Gasparini, C. J. Brabec, D. Baran and I. McCulloch, *Chem. Soc. Rev.*, 2019, **48**, 1596–1625.

34 W. Wagner, M. Wehner, V. Stepanenko and F. Würthner, *J. Am. Chem. Soc.*, 2019, **141**, 12044–12054.

35 E. Zhou, J. Cong, Q. Wei, K. Tajima, C. Yang and K. Hashimoto, *Angew. Chem., Int. Ed.*, 2011, **50**, 2799–2803.

36 P. M. H. Kazmaier and R. Hoffmann, *J. Am. Chem. Soc.*, 1994, **116**, 9684–9691.

37 S. K. Mohan Nalluri, J. Zhou, T. Cheng, Z. Liu, M. T. Nguyen, T. Chen, H. A. Patel, M. D. Krzyaniak, W. A. Goddard 3rd, M. R. Wasielewski and J. F. Stoddart, *J. Am. Chem. Soc.*, 2019, **141**, 1290–1303.

38 Y. Yu, Q. Shi, Y. Li, T. Liu, L. Zhang, Z. Shuai and Y. Li, *Chem. – Asian J.*, 2012, **7**, 2904–2911.

39 H.-M. Zhao, J. Pfister, V. Settels, M. Renz, M. Kaupp, V. C. Dehm, F. Würthner, R. F. Fink and B. Engels, *J. Am. Chem. Soc.*, 2009, **131**, 15660–15668.

40 M. J. Lin, A. Jimenez, C. Burschka and F. Wurthner, *Chem. Commun.*, 2012, **48**, 12050–12052.

41 F. Schlosser, V. Stepanenko and F. Wurthner, *Chem. Commun.*, 2010, **46**, 8350–8352.

42 A. D. Shaller, W. Wang, H. Y. Gan and A. D. Q. Li, *Angew. Chem., Int. Ed.*, 2008, **47**, 7705–7709.

43 Á. J. Jiménez, M.-J. Lin, C. Burschka, J. Becker, V. Settels, B. Engels and F. Würthner, *Chem. Sci.*, 2014, **5**, 608–619.

44 M. M. Safont-Sempere, P. Osswald, K. Radacki and F. Würthner, *Chem. – Eur. J.*, 2010, **16**, 7380–7384.

45 M. M. Safont-Sempere, P. Osswald, M. Stolte, M. Grune, M. Renz, M. Kaupp, K. Radacki, H. Braunschweig and F. Würthner, *J. Am. Chem. Soc.*, 2011, **133**, 9580–9591.

46 W. Wang, L. S. Li, G. Helms, H. H. Zhou and A. D. Q. Li, *J. Am. Chem. Soc.*, 2003, **125**, 1120–1121.

47 W. Wang, W. Wan, H. H. Zhou, S. Q. Niu and A. D. Q. Li, *J. Am. Chem. Soc.*, 2003, **125**, 5248–5249.

48 L. L. Crowe, K. M. Solntsev and L. M. Tolbert, *Langmuir*, 2007, **23**, 6227–6232.

49 W. Zhang, X. Zhou, Z. Xie, B. Yang, L. Liu and Y. Ma, *Chem. Commun.*, 2013, **49**, 11560–11562.